ROBERT KOCH INSTITUT

Originally published as:

Mahrhold, S., Bergström, T., Stern, D., Dorner, B.G., Åstot, C., Rummel, A.
Only the complex N559-glycan in the synaptic vesicle glycoprotein 2C mediates high affinity binding to botulinum neurotoxin serotype A1
(2016) Biochemical Journal, 473 (17), pp. 2645-2654.

DOI: 10.1042/BCJ20160439

This is an author manuscript.
The definitive version is available at: http://www.biochemj.org/content/early/2016/06/16/BCJ20160439

Only the complex N559-glycan in the synaptic vesicle glycoprotein 2C mediates high affinity binding to botulinum neurotoxin serotype A1

Stefan MAHRHOLD*, Tomas BERGSTRÖM†, Daniel STERN‡, Brigitte G. DORNER‡, Crister ÅSTOT† and Andreas RUMMEL*[1]

* Institut für Toxikologie, Medizinische Hochschule Hannover, Carl-Neuberg-Str. 1, 30625 Hannover, Germany
† Division for CBRN Defence and Security, Swedish Defence Research Agency, Cementvägen 20, 90182 Umeå, Sweden
‡ Biological Toxins, Centre for Biological Threats and Special Pathogens, Robert Koch Institute, Seestr. 10, 13353 Berlin, Germany

[1]To whom correspondence should be addressed (email: rummel.andreas@mh-hannover.de)

Synopsis: The extraordinary potency of botulinum neurotoxins (BoNTs) is mediated by their high neurospecificity, targeting peripheral cholinergic motoneurons leading to flaccid paralysis and successive respiratory failure. Complex polysialo gangliosides accumulate BoNTs on the plasma membrane and facilitate subsequent binding to synaptic vesicle membrane proteins which results in toxin endocytosis. The luminal domain 4 (LD4) of the three synaptic vesicle glycoprotein 2 (SV2) isoforms A-C mediates uptake of the clinically most relevant serotype BoNT/A. SV2C-LD4 exhibits the strongest protein-protein interaction and comprises five putative N-glycosylation sites. Here, we expressed human SV2C-LD4 fused to human IgG-Fc in prokaryotic and eukaryotic expression systems to analyse the effect of N-glycosylation of SV2C on the interaction with BoNT/A. Mass spectrometric analysis of gSV2CLD-Fc demonstrates glycosylation of N534, N559 and N565, the latter two residing at the BoNT/A interface. Mutational analysis exhibits that only the N559-glycan, but not N565-glycan increases affinity of BoNT/A to human gSV2C-LD4. The N559-glycan was characterised as of complex core-fucosylated type with a heterogeneity ranging up to tetra-antennary structure with bisecting N-acetylglucosamine which can establish extensive interactions with BoNT/A. The mutant gSV2CLD-Fc N559A displayed a 50-fold increased dissociation rate k_d resulting in an overall 12-fold decreased binding affinity in surface plasmon resonance experiments. The delayed dissociation might provide BoNT/A more time for endocytosis into synaptic vesicles. In conclusion, we show the importance of the complex N559-glycan of SV2C-LD4, adding a third anchor point beside a ganglioside and the SV2C-LD4 peptide, for BoNT/A neuronal cell surface binding and uptake.

Short title: Complex N559-glycan of SV2C mediates high affinity to BoNT/A

Key words: botulinum neurotoxin A, synaptic vesicle glycoprotein 2C, N-glycan, HEK cell expression, surface plasmon resonance, LC-MS/MS

Abbreviations used: BoNT, botulinum neurotoxin; Fc, homodimer of second and third constant domains of IgG heavy chains (fragment crystallisable); GBS, ganglioside binding site; HC, heavy chain; H_C, C-terminal fragment of the HC; H_{CC}, C-terminal domain of H_C; H_{CN}, N-terminal domain of H_C-fragment; H_CE, H_C of BoNT serotype E; H_CA, H_C of BoNT serotype A; LC, light chain; LC-MS/MS, liquid chromatography tandem mass spectrometry; PNG, putative N-glycosylation site; NGS, N-glycosylation site; NMJ, neuromuscular junction; SV2, synaptic vesicle glycoprotein 2; Syt, synaptotagmin; tetanus neurotoxin TeNT.

INTRODUCTION

The family of botulinum neurotoxins consists of seven established serotypes termed A to G (BoNT/A-G) which are the etiologic agents of the neuromuscular disease botulism. Their extreme potency, the ubiquitous presence of *Clostridium botulinum* spores and the high mortality rate of untreated botulism led to the declaration of BoNTs as category A select agents [1, 2] and as a potential weapon of bioterrorism. Nevertheless, especially BoNT/A and B are successful, licensed drugs to treat an ever-growing number of medical and cosmetic conditions which are characterized by hyperactivity of peripheral synapses [3]. The BoNTs are bacterial protein toxins of the AB-type that are synthesized as a single polypeptide chain which becomes proteolytically activated by bacterial or host proteases to form a 100 kDa heavy chain (HC) and a 50 kDa light chain (LC). In the active di-chain toxin, both chains remain associated by a single disulphide bond [4]. The LC, a Zn^{2+}-dependent metalloprotease, represents the enzymatically active part A and specifically cleaves members of the SNARE-family of proteins which are indispensable for the neurotransmission at synapses. Their cleavage halts the neuroexocytosis of acetylcholine at the neuromuscular junction (NMJ), which leads to a flaccid paralysis of the affected muscle and hence to symptoms of botulism. Since the HC mediates the binding and uptake of the LC into target cells, it represents the binding part B. It consists of the 50 kDa amino-terminal translocation (H_N) and the 50 kDa carboxyl-terminal cell-binding domain (H_C). H_N is supposed to form a channel in the membrane of the acidifying endosome, which allows the transport of the LC through the endosomal membrane into the target cell cytosol [5, 6]. The H_C mediates binding to target cells and consists of the 25 kDa amino-terminal H_{CN} and the 25 kDa carboxyl-terminal H_{CC} domain [7].

The extreme potency of BoNTs is predominantly due to their specific interaction with the presynaptic membrane at NMJs. It was shown that complex polysialo gangliosides accumulate the toxin molecules via their H_{CC} domain in the plane of the plasma membrane with sub-micromolar affinity [7]. In case of BoNT/A, a single ganglioside binds with its terminal GalNAc-Gal moiety into a ganglioside binding site (GBS) comprising a residue motif also largely conserved in BoNT/B, E, F, G and tetanus neurotoxin (TeNT) [8-10]. Enriching the BoNT in the two-dimensional plane of the presynaptic membrane considerably facilitates the subsequent interaction with a second receptor which leads to an activity-dependent, receptor-mediated uptake of the toxin into small synaptic vesicles. Accordingly, BoNT/B, G and mosaic type BoNT/DC employ the luminal domain (LD) of the synaptic vesicle transmembrane proteins synaptotagmin-I and -II as protein receptor [11-14]. BoNT/A interacts with the fourth large luminal domain (LD4) of the synaptic vesicle glycoprotein 2 isoforms A-C (SV2A-C). The SV2s are integral, rare (1-2 copies per SV, [15]) proteins residing in the membrane of synaptic vesicles. They are predicted to span the vesicle membrane twelve times (Figure 1A). The LD4 between transmembrane regions seven and eight is about 125 amino acids long, glycosylated and becomes extracellularly exposed upon neuroexocytosis (Figure 1A)[16]. Also BoNT/E binds the LD4 of SV2A and SV2B as second receptor [17-19] while the exact molecular mechanism how BoNT/D, F and the closely related TeNT use SV2A-C during their uptake process [10, 20-22] is unknown, because no direct interaction between SV2 and BoNT/D, F or TeNT has yet been demonstrated. Initially, TeNT binds the extracellular matrix proteins nidogen-1 and -2 (also known as entactins) as receptors at the NMJ [23]. Above all, no protein receptor has been identified for BoNT/C, but it was proposed instead that this serotype enters neurons only by binding to two ganglioside molecules [24].

It was demonstrated that BoNT/A binds *E. coli*-expressed, non-glycosylated SV2C-LD4 much stronger compared to non-glycosylated SV2A- and SV2B-LD4 [17, 19, 25]. Recently, the crystal structure of H_CA in complex with non-glycosylated human SV2C-LD4 was solved [26]. Here, SV2C-LD4 forms a right-handed, quadrilateral β-helix which associates with H_CA mainly via backbone-backbone interactions and only a few side chain interactions at the opposite site of the single GBS in H_{CC} close to the H_{CN} (Figure 1B-C). In parallel, mutational analysis also allocated the SV2 binding site opposite of the single GBS in $H_{CC}A$, but additionally identified functional residues outside the protein-protein interface [27] which could interact with posttranslational modifications of SV2. It is known that the LD4 of SV2 is glycosylated [16] and that the LD4 of SV2A, B and C contain three, three and five putative N-glycosylation (PNG) sites, respectively, based on the motif N-X-S/T (X can be any amino acid except proline). It was demonstrated that BoNT/E, in contrast to BoNT/A, only exploits glycosylated SV2A and B as cellular receptors. In particular, BoNT/E strictly requires glycosylation of N573 in SV2A to be able to bind and to enter target cells [18, 28]. A similar role of N573 in SV2A for binding of BoNT/A was postulated, but has not been unambiguously demonstrated [18]. No work about the contribution of N-glycans in SV2C-LD4 to the interaction with BoNT/A has been published so far.

Here, we determined the binding kinetics of BoNT/A to glycosylated SV2C-LD4, identified the N559-glycan in glycosylated SV2C-LD4 as main factor mediating the high affinity interaction with BoNT/A, and characterized the N559-glycan as mainly tetra-antennary, core-fucosylated structure partly equipped with a bisecting N-acetylglucosamine (GlcNAc).

EXPERIMENTAL

Chemicals and reagents

Methanol and acetonitrile (LC-MS grade) were purchased from Merck, Germany, formic acid (MS grade) from Fluka, Switzerland, DTT, iodoacetamide (IAM) and ammonium bicarbonate from Sigma-Aldrich (USA), porcine trypsin of sequencing grade from Promega, USA and water from a Milli-Q system, Merck, Germany.

Construction of plasmids

The plasmid pIg+H6thSV2CLDS, facilitating the eukaryotic expression and secretion of the glycosylated human SV2C-LD4 (gSV2CLD) fused C-terminally to human IgG1-Fc (gSV2CLD-Fc), was generated by cloning a synthetic *E. coli* codon usage optimized DNA sequence encoding hSV2C-455-579 [25] equipped with N-terminal His6- and C-terminal Strep-tag (IBA GmbH) to allow tandem affinity purification into the *Eco*R V and *Xba* I sites between the CD33 signal peptide and the hIgG1-Fc sequence of the plasmid pIg+ (R&D Systems). The plasmid pH6thSV2CLDSFc, facilitating the prokaryotic expression of non-glycosylated SV2CLD-Fc, was generated by amplification of the corresponding DNA sequence omitting the CD33 signal peptide and His6-tag sequences by means of PCR using pIg+H6thSV2CLDS as template and appropriate oligonucleotides. The resulting DNA fragment was cloned into the *Bam*H I and *Hind* III sites of pH6thSV2C 455-579 [25]. All mutations were introduced using the GeneTailor Mutagenesis System (life technologies) and the nucleotide sequences of all constructs and mutants were verified by DNA sequencing (GATC Biotech, Germany).

Purification of recombinant proteins

Recombinant H_CA comprising a C-terminal Streptag and full-length, tag-free, di-chain BoNT/A have been expressed and purified as previously described [8, 29]. gSV2CLD-Fc was purified from cell culture supernatants of transiently transfected HEK293T cells. Briefly, one day before transfection 18×10^6 cells were seeded in 300 cm² culture flasks using growth medium (DMEM (Sigma, D5671) supplemented with 10% FCS (PAN Biotech, P30-1502), 10 U mL^{-1} penicillin, 100 µg mL^{-1} streptomycin and 2 mM L-glutamine). Transfection was performed by exchanging the growth medium of the culture and incubating 32 µg pIg+H6thSV2CLDS and 92 µL branched polyethylenimine (1 mg mL^{-1}, Sigma, #408727) in 4 mL DMEM without serum. Following 20 min of incubation at room temperature the mixture was added to the culture. Transfection efficiency was estimated by replacing one-tenth of the amount of the DNA with the plasmid pEGFP-N2 (BD Biosciences Clontech) and visual inspection of the green fluorescence of the cells one day after transfection. Following this protocol the transfection efficiency was typically approximately 60%. Cell culture supernatants were collected two, four and six days after transfection. Non-glycosylated SV2CLD-Fc was purified from lysates of transformed *E. coli* strain M15 [pREP4] (Qiagen), following 16-18 h of induction with 0.2 mM IPTG at 21°C.

gSV2CLD-Fc and SV2CLD-Fc were consecutively affinity purified on Talon matrix (Clontech) and Streptactin-Superflow (IBA GmbH) columns according to the manufacturers' instructions. Both fusion proteins were eluted using 100 mM Tris–HCl (pH 8.0), 150 mM NaCl and 10 mM Desthiobiotin. Fractions containing high amounts of protein were pooled, shock-frozen in liquid nitrogen and kept frozen at -70°C until usage. Protein concentrations were determined by densitometry following SDS-PAGE and Coomassie Blue staining using various known concentrations of bovine serum albumin (BSA) as standards.

SV2C Binding Assay

Binding of wild-type and mutant gSV2CLD-Fc and SV2CLD-Fc to H_CA and BoNT/A, respectively, was carried out in binding buffer (20 mM Tris-HCl, pH 7.4, 150 mM NaCl and 0.5% Triton X-100). A total of 10 µL protein G-sepharose beads (GE Healthcare) coated with 100 pmol of gSV2CLD-Fc or non-glycosylated SV2CLD-Fc was incubated with the indicated concentrations of H_CA or BoNT/A, respectively, for 2-3 h in a total volume of 200 µL. Following incubation, beads were collected by centrifugation at 4500 × g and washed three times using binding buffer. Washed pellet fractions were incubated in sodium dodecyl sulphate (SDS) sample buffer for 5 min at 99°C and analyzed by SDS-PAGE. Proteins were visualized by means of Coomassie Blue staining.

LC-MS and LC-MS/MS analysis

gSV2CLD-Fc protein samples were precipitated using ice-cold methanol as described elsewhere [30]. The precipitated proteins were reduced by addition of 20 µL 10 mM DTT/80 mM ammonium bicarbonate solution (60°C, 60 min) followed by alkylation in darkness (30°C, 40 min) after addition of 2 µL 150 mM IAM solution (final conc. 15 mM, ~pH 8). Sample digestion (45°C, 60 min) was performed after adding 2 µL of a 0.2 µg/µL trypsin solution. The obtained peptides were acidified, diluted and analysed by LC-MS and MS/MS on a Waters Nano-Acquity UPLC system connected to a Waters QTOF Ultima mass spectrometer equipped with a nano-electrospray ion source (Waters Corporation, Milford, USA). The peptides were separated on a 150 mm BEH C18 nanoAcquity UPLC column (Waters) using a water:acetonitrile gradient containing 0.1% formic acid from 3-40% over 25 min at a flow rate of 400 nL min^{-1}. Samples were screened for glycopeptide content in LC-MS mode using collision energies (CEs) ranging from 6-40 eV with argon as the collision target. Glycopeptides were analysed in terms of sugar content using LC-MS/MS of selected precursors.

Surface plasmon resonance (SPR) measurements

Binding kinetics and affinity were determined on a Biacore X100 unit (GE Healthcare) at 25°C using phosphate buffered saline (PBS, pH 7.3) supplemented with 0.5% Triton X-100 as running buffer. To this aim, a mouse anti-human IgG-Fc-specific monoclonal antibody was covalently coupled to a CM5 sensor chip according to manufacturer's instructions (Human IgG Capture Kit; GE Healthcare). gSV2CLD-Fc wild-type and N559A mutant (10 µg mL^{-1}) were immobilized for 120 seconds at a flow rate of 5 µL min^{-1} on flow cell 2 by a capture approach via the C-terminal human IgG1-Fc-portion to a mean surface density of 317 resonance units (RU). Recombinant H_CA was injected for 60 seconds over both flow cells at a flow rate of 30 µL min^{-1} to monitor binding association followed by 300 seconds injections of running buffer to monitor binding dissociation. Between measurements, the sensor chip was regenerated by injections of 3 M $MgCl_2$ for 30 seconds at 20 µL min^{-1}. Each measurement cycle consisted of injections of 1:3 serial dilutions of recombinant H_CA ranging from 1800 nM to 22.2 nM with duplicate injections of the highest concentration and triplicate injections of buffer only. The kinetic association rate constants k_a, the dissociation rate constants k_d and the equilibrium binding constants K_D were determined by fitting a 1:1 Langmuir interaction model with RI set to 0 and R_{max} fitted globally to the double referenced [31] binding curves using the Biacore Evaluation Software 2.01 or the BIAevaluation Software 4.1.1 (GE Healthcare).

RESULTS

Luminal domain 4 of SV2C comprises five putative N-glycosylation sites

Sequence comparison of the LD4s of all three SV2 isoforms of mouse, rat and human origin revealed the presence of three conserved PNG sites (Figure 1 and S1). In human SV2C (hSV2C), these sites are N484, N534 and N559. However, compared to the SV2A & B isoforms SV2C displays two additional unique PNG sites at N480 and N565 (Figure 1 and S1), suggesting that SV2C contains two additional N-glycans. Indeed, gSV2CLD-TD migrates at higher molecular weight in SDS-PAGE than gSV2ALD-TD [28].
Previous studies demonstrated that the glycosylation of the third conserved N573 in SV2A is a prerequisite for the interaction with BoNT/E [18]. Interestingly, our inspection of the crystal structure of H_CA in complex with non-glycosylated hSV2C-LD4 [26] revealed that the corresponding third conserved PNG site in hSV2C (N559) as well as the non-homologous PNG site at N565 are localized in very close proximity to H_CA whereas the remaining three PNG sites either point away (N534) or are too far from the H_CA surface (N480, N484; Figure 1B). Therefore, it was reasonable to assume that most likely the sugar moieties of N-glycans attached to N559 or N565 in SV2C would mediate additional interactions between SV2C and H_CA. These additional interactions were hypothesized to translate into a higher affinity and/or different binding kinetics of H_CA to glycosylated compared to non-glycosylated SV2C.

gSV2CLD-Fc is secreted as soluble protein

To test our hypothesis, we expressed hSV2C-LD4 fused to human IgG-Fc in HEK cells to obtain glycosylated gSV2CLD-Fc (Figure 2A). Subsequently, several mutations were introduced to disable glycosylation of N559 and/or N565, respectively. In order to unambiguously discriminate between effects elicited by the exchange of the amino acid side chains and effects caused by the loss of the corresponding N-glycan, we additionally expressed the fusion proteins in a bacterial expression system to generate glycan-free SV2CLD-Fc.
Sufficient amounts of soluble gSV2CLD-Fc fusion proteins (Figure 2A) were obtained from culture supernatants of transiently transfected HEK293T cells, indicating that the gSV2CLD-Fc becomes readily secreted into the culture medium. Affinity purified gSV2CLD-Fc appeared as a diffuse array of bands with an apparent molecular weight of around 60 kDa in SDS-PAGE (Figure 2B), which clearly exceeds the calculated molecular weight of approximately 46 kDa for the SV2CLD polypeptide chain. Hence we conclude that the proteins are glycosylated upon expression in HEK cells. The mass of N-glycan ranges from 892 Da of the common core structure subunit $GlcNAc_2Man_3$ to >3500 Da of a complex sialylated, core-fucosylated, tetra antennary structure. On average, the 15 kDa molecular weight increase agrees well with the presence of 4-6 N-glycans in gSV2CLD-Fc. The diffuse appearance of the protein bands is probably caused by the observed micro heterogeneity of some of the N-glycans. Both the mutation of the fourth (N559A, N559Q and S561A) or the fifth (N565Q) PNG of gSV2CLD-Fc resulted in an increased mobility of the mutant in SDS-PAGE compared to gSV2CLD-Fc wild-type, indicating that both sites are N-glycosylated (Figure 2B). Furthermore, the double mutant gSV2CLD-Fc N559Q/N565Q showed an even stronger increase in mobility, confirming the simultaneous glycosylation of both sites in HEK cells. In addition, N-glycosylation of N534, N559 and N565 in SV2CLD and of N297 in the IgG-Fc peptide EEQY**N**STYR was confirmed by LC-MS analysis of trypsin digestion derived peptides of gSV2CLD-Fc wild-type. The identified N-glycosylated

SV2C peptides are summarized in Table 1 and the corresponding data for single mutants gSV2CLD-Fc N559Q and N565Q are included as supplementary information (Table S1). Non-glycosylated SV2CLD-Fc constructs were purified from *E. coli* cell lysates and, as expected, migrated as discrete band corresponding to ~46 kDa. Here, no differences in mobility were visible between SV2CLD-Fc wild-type and SV2CLD-Fc mutants (Figure 3B).

The N559-glycan increases affinity of gSV2CLD-Fc to BoNT/A

To analyse the influence of the N-glycans attached to N559 and N565 on the interaction of SV2C with BoNT/A, purified gSV2CLD-Fc and glycan-free SV2CLD-Fc fusion proteins were immobilized to protein G-sepharose beads to precipitate isolated H_CA or BoNT/A from solution. BoNT/A had to be used as an alternative ligand for hSV2CLD-Fc because H_CA exhibits a similar mobility as SV2CLD-Fc which would have impeded the analysis of the bound proteins by SDS-PAGE.
Wild-type gSV2CLD-Fc and SV2CLD-Fc showed robust binding to H_CA and BoNT/A, respectively (Figure 3A and B). Also the single mutant gSV2CLD-Fc N565Q exhibited binding to H_CA indistinguishable from gSV2CLD-Fc wild-type, indicating that neither the N565-glycan nor the amino acid N565 itself contributes to the interaction with BoNT/A (Figure 3A, left panel). In contrast, the single mutant gSV2CLD-Fc N559Q displayed clearly reduced affinity to BoNT/A (Figure 3A). Accordingly, simultaneous mutation of N559Q and N565Q did not reduce binding any further compared to gSV2CLD-Fc N559Q, again confirming that neither the N565-glycan nor N565 itself contributes to the interaction with BoNT/A (Figure 3A, left panel). Hence, mutant N565Q was excluded from further analysis, while mutant SV2CLD-Fc N559Q was additionally expressed in *E. coli* to verify the effect of the elongated side chain of Q559 (Figure 1C and 3B) on the binding to BoNT/A. Surprisingly, also SV2CLD-Fc N559Q displayed decreased affinity to BoNT/A compared to SV2CLD-Fc wild-type indicating a negative influence of the elongated amide side chain. In silico substitution of N559Q reveals that the H-bonds between the amide group of N559 and T1145/Y1149 of BoNT/A [26] are lost and an interference of the amide group of Q559 with the phenyl ring of F953 might arise due to insertion of the methylene group (Figure 1C). Since the glycosylated and non-glycosylated N559Q mutants both show a reduced binding, the observed negative effect can be attributed to the perturbation by glutamine as well as to the missing N559-glycan. Hence the N559Q mutation is not suitable to discriminate between the effect caused by the missing N559-glycan and the effect on protein-protein interaction.
Therefore we tried to prevent glycosylation of N559 by exchanging S561 of the PNG motif N-X-S/T to alanine. Indeed, the gSV2CLD-Fc S561A mutant exhibited an increased mobility in SDS-PAGE compared to wild-type, indicating the absence of the N559-glycan (Figure 2B). However, gSV2CLD-Fc S561A as well as SV2CLD-Fc S561A displayed reduced binding to H_CA (Figure 3A) and BoNT/A (Figure 3B), respectively. Here, lack of N559-glycan as well as lack of the S561 hydroxyl group establishing water mediated H-bonds with the amide and carbonyl groups of R1294 and the carboxyl group of E1293 of H_CA (Figure 1C) impair binding. Hence, S561 cannot be modified without affecting the protein-protein interaction and also does not allow analysis of N559 glycosylation on BoNT/A binding.
Although the amide group of N559 displays H-bonds to T1145 and Y1149 of BoNT/A [26] we then generated the mutant SV2CLD-Fc N559A (Figure 2). Surprisingly, SV2CLD-Fc N559A exhibited no effect on binding to BoNT/A confirming previous biochemical data by Benoit et al. (Figure 3B,), but also suggesting that N559 backbone interactions are by far more important than its side chain H-bonds. Like gSV2CLD-Fc N559Q also gSV2CLD-Fc N559A showed an increased mobility in SDS-PAGE indicating absence of the N559-glycan. Finally, gSV2CLD-Fc N559A exhibited a strong reduction in binding to H_CA (Figure 3A,

right panel) compared to gSV2CLD wild-type, demonstrating the importance of N559-glycan for high affinity binding to BoNT/A.

N559-glycan drastically decreases dissociation of H_CA from gSV2CLD-Fc as shown by surface plasmon resonance

To validate the increased binding of BoNT/A to gSV2CLD-Fc and to determine the influence of the N559-glycan on binding affinity and kinetics, we employed SPR measurements. To mirror the natural presentation of the SV2C-LD4, gSV2CLD-Fc wild-type and the three gSV2CLD-Fc mutants N559A, N559Q and S561A served as receptors and were captured employing the Fc-portion via an immobilized anti-human-IgG capture antibody. Recombinant H_CA was injected as analyte in a concentration range from 1800 nM to 22.2 nM and kinetic binding rates were determined by fitting the measured interactions to a 1:1 Langmuir binding model. Only mutant gSV2CLD-Fc S561A required fitting to the heterogeneous binding model (Table 2; Figure 4 and S2).
In agreement with the binding assay, we also observed much stronger binding of H_CA to gSV2CLD-Fc wild-type as compared to all three gSV2CLD-Fc mutants. E.g., the overall affinity is 12-fold higher than to gSV2CLD-Fc N559A mainly due to a ~50-fold decreased dissociation rate k_d of H_CA from gSV2CLD-Fc wild-type (Table 2). On the contrary, the about 4-fold reduced association rate of H_CA to the gSV2CLD-Fc wild-type might be explained by the spatial constraint introduced by the additional interaction of the N559-glycan requiring the carbohydrates to correctly orient for interaction with H_CA. gSV2CLD Fc N559A and N559Q display identical binding kinetics (fast association and dissociation typical for constructs lacking the N559-glycan) and a similar binding constants (Figure 4 and S2). gSV2CLD Fc S561A exhibits a heterogeneous binding of H_CA, but again the dominating component describes fast association and dissociation of H_CA which is characteristic of a transient SV2C peptide interaction (Figure S2).
In conclusion, SPR-measurements delivered a mechanistic explanation for the increased affinity of BoNT/A binding to glycosylated SV2C by showing that the additional interaction with the N559-glycan stabilizes the complex by introducing an additional interaction site.

N559 holds a tetra antennary, core-fucosylated N-glycan with a bisecting GlcNAc

The gSV2CLD-Fc N559Q and gSV2CLD-Fc N565Q mutants were initially used to identify the N-glycans present in gSV2CLD-Fc wild-type. The glycan identification in the single mutants made use of the glycan heterogeneity in the expressed proteins, including a small fraction of non-glycosylated tryptic peptides. Thus, the non-glycosylated $Q^{559}C^*SFFHNK^{566}$ (C*=carbamidomethylated cysteine) and $N^{559}C^*SFFHQK^{566}$ peptides were identified in the mutants gSV2CLD-Fc N559Q and gSV2CLD-Fc N565Q, respectively. Figure S3 displays LC-MS chromatograms of these non-glycosylated peptides together with the wild-type analogue. Glycosylation of peptides has a limited effect on their hydrophilic properties, and consequently the non-glycosylated peptides indicated the retention time of interest for corresponding glycopeptides. The retention times were used in combination with LC-MS analysis at high collision energy to uncover the corresponding glycopeptides $Q^{559}C^*SFFHN_{glyco}K^{566}$ and $N^{559}{}_{glyco}C^*SFFHQK^{566}$ in gSV2CLD-Fc N559Q and gSV2CLD-Fc N565Q, respectively. Diagnostic carbohydrate fragment ions (m/z 204.1 and 366.1) produced at high collision energy [32] were used for the glycopeptide identification. Both of the two peptides were N-glycosylated and showed a high degree of glycan heterogeneity. The glycan moiety at N559 in the gSV2CLD-Fc N565Q mutant was expected

to suppress the trypsin digestion at the N-terminal K558/N559-trypsin cleavage site and indeed the intensities of the two almost identical Q-mutant peptides were very different (data not shown). This suppression of K558/N559-cleavage increased the intensity of the longer $F^{552}IDSEFKN_{glyco}C^{*}SFFHQK^{566}$ peptide and the corresponding double glycosylated peptide $F^{552}IDSEFKN_{glyco}C^{*}SFFHN_{glyco}K^{566}$ was identified in the gSV2CLD-Fc wild type construct. Thus, the N559- and N565-glycans of gSV2CLD-Fc wild-type were confirmed in both the short $N^{559}{}_{glyco}C^{*}SFFHN_{glyco}K^{566}$ peptide (Table 1) and in the longer $F^{552}IDSEFKN_{glyco}C^{*}SFFHN_{glyco}K^{566}$ peptide (Figure 6, Table 1) produced by one missed trypsin cleavage site. A summary of identified peptides and glycopeptides within the sequence of interest is shown in Table 1 (for gSV2CLD-Fc wild-type) and in Table S1 (for gSV2CLD-Fc N559Q and gSV2CLD-Fc N565Q mutants).

LC-MS/MS analysis of the glycosylated $F^{552}IDSEFKN_{glyco}C^{*}SFFHQK^{566}$ peptide derived from the gSV2CLD-Fc N565Q mutant which showed BoNT/A binding indistinguishable from gSV2CLD-Fc wild-type revealed the detailed N559-glycan structure. At intermediate collision energy the losses of terminal galactoses (Gals) and GlcNAcs were detected (Figure 5, top panel). At higher collision energy, subsequent fragmentation of tri-mannose (Man_3), fucose (Fuc) and GlcNAc core structures were observed (Figure 5, lower panel). Based on the data the presence of a tetra antennary, core-fucosylated N-glycan type was concluded. In addition, LC-MS data of the peptide verified a bisecting GlcNAc (Table S1). LC-MS analysis of the gSV2CLD-Fc wild-type showed glycan heterogeneity at N559 and N565. Both sites carry core-fucosylated N-glycans ranging from dual (~15%), tri (~39%) to tetra antennary (~45%) structures of the total glycan pool. About 13% of the tetra antennary structures also contain a bisecting GlcNAc (Figure 6).

DISCUSSION

Botulinum neurotoxins exploit the recycling pathway of synaptic vesicles to gain access to the cytosol of peripheral cholinergic motoneurons. To this end, BoNTs interact with luminal segments of transmembrane proteins of synaptic vesicles which temporarily become exposed to the synaptic cleft upon exocytosis of neurotransmitter [7]. The luminal segments of most of these proteins including synaptotagmin and synaptic vesicle glycoprotein 2 are known to be multiply glycosylated [16, 33, 34]. Nonetheless, the interaction of BoNT/A with SV2C was first discovered and characterized using *E. coli*-expressed non-glycosylated luminal domain of SV2C [17, 19], demonstrating sufficient affinity of BoNT/A to the bare SV2C peptide to detect robust binding *in vitro*. However, expressing the luminal domain of human SV2C fused to human IgG Fc in HEK cells, we were able to isolate secreted glycosylated gSV2CLD-Fc. MS analysis could detect N-glycosylation at the three C-terminal of the five putative PNG sites. Subsequently, we unambiguously demonstrated that the N559-glycan strengthens the binding of BoNT/A to SV2C 12-fold.

N-glycan patterns can vary from tissue to tissue, between cell types or even depending on the localisation/organelle or the developmental stage of the organism. Few studies (e.g. [35, 36]) analysed sialylated N-glycans of brain homogenate. However, apart from the use of CNS tissue instead of PNS also a complex mixture of different neurons and other accompanying cells was analysed and does not reflect the true situation BoNT/A will face at the motoneuron. Since we expressed SV2C in non-neuronal HEK cells, we could not expect to obtain the exact, yet unknown, N-glycosylation pattern of native SV2C which might even differ between SV2C being expressed in central or peripheral neurons. Nevertheless, our HEK cell-expressed gSV2CLD-Fc supported high affinity binding of BoNT/A with a K_D of 110 nM. In contrast, mutant gSV2CLD-Fc N559A lacking the N559-glycan displayed a 12-fold reduced affinity. Looking at the co-crystal structure of *E. coli*-expressed non-glycosylated SV2C in complex with H_CA [26], the side chain of N559 points towards a crevice in H_CA formed by the amino acids G1292, F953, Y1149 and T1145 which could accommodate the proximal core sugars of the N559-glycan. In contrast, residue N565, also close to the H_CA surface, points away from the binding interface and is not offered a similar crevice on H_CA, thereby explaining the observation that mutation of this residue did not alter the BoNT/A-SV2C interaction at all. Mutants gSV2CLD-Fc N559Q and S561A also devoid of the N559-glycan showed similarly decreased binding to H_CA, respectively, but the bacterial expressed, non-glycosylated SV2CLD-Fc N559Q and S561A also exhibited reduced affinity to BoNT/A preventing a clear-cut conclusion about the role of the N559-glycan in BoNT/A recognition. However, SV2CLD-Fc N559A bound BoNT/A indistinguishable from SV2CLD-Fc wild-type thereby unambiguously demonstrating the important role of N559-glycan in BoNT/A recognition. The function of the N559-glycan is reminiscent of the BoNT/E-SV2A interaction which is facilitated by the presence of an N-glycan attached to the homologous residue N573 [18]. Whether the N573Q mutation in SV2A used by Dong et al. negatively influences the already weak SV2A-BoNT/E protein-protein interaction cannot be revealed, because it is impossible to detect binding of BoNT/E to *E. coli*-expressed non-glycosylated SV2ALD *in vitro* [17, 19]. However, conclusions drawn that the N573-glycan also contributes to BoNT/A binding and uptake by using the SV2A N573Q mutant [18] are ambiguous because we demonstrated a negative impact on the BoNT/A-SV2C protein-protein interaction by a glutamine at the homologous position 559.

Kinetic analysis demonstrates that N559-glycan clearly increases affinity of SV2C towards BoNT/A. The known affinity of BoNT/A towards bacterial SV2C suggests that the protein-protein interaction controls the overall binding mechanism by initiating the binding process. Subsequently, the N559-glycan is able to bury in the neighbouring crevice via multiple non-covalent interactions which on one hand decreases the association rate k_a 4-fold, but on the

other hand reduces the dissociation rate k_d of H_CA 50-fold. In other words, the residence time of BoNT/A, bound in a trivalent fashion to a single ganglioside, the SV2C protein backbone and its N559-glycan, is sufficiently extended to allow its efficient endocytosis upon recycling of the SV. A similar mechanism can be postulated also for the other SV2 binders BoNT/E and F. However, in their case N-glycosylation is much more crucial since the protein-protein interactions between BoNT/E and F with SV2A-C are very weak, even preventing the demonstration of binding to bacterial expressed SV2A-C LD4 [17, 19]. The observation that BoNT/E exhibits an expanded bipartite interface for the interaction with SV2A [28] which differs significantly from the SV2C binding site of BoNT/A [27] might compensate the weak protein-protein interaction.

Previously, the identification and characterisation of the SV2C binding site of BoNT/A by means of site-directed mutagenesis [27] identified residues which retrospectively do not directly interact with amino acids of SV2C according to the SV2C-H_CA co-crystal structure [26]. Explicitly, mutation of the amino acids N905, F917, T1063, H1064, D1108, V1287 and G1292 interfered with the neurotoxicity of BoNT/A in the mice phrenic nerve hemidiaphragm assay, e.g. mutant G1292R showed a 350-fold reduction of neurotoxicity [27]. A structural explanation for this observation might be that the large arginine residue blocks the core structure of the N559-glycan from entering its binding site. The other residues are located further away from the crevice near G1292 up to a groove on the surface of $H_{CC}A$. Aromatic residues like F917 and H1064 are well known to interact with the hydrophobic face of the carbohydrates, whereas polar residues like N905, T1063 and D1108 might form H-bonds with the sugars' hydroxyl groups. ND2 of N559 in SV2C is 18 Å, 21 Å and 29 Å away from F917, N905 and D1108, respectively. The distance between the ND2 of N314 in human IgG and its terminal Man in the common core structure subunit ranges from 18-20 Å [37]. The subsequent GlcNAc adds another 5 Å. Complex N-glycan types are expected to extend up to 30 Å out from the N559 residue and will occupy a large volume as calculated for similar glycan structures [38]. Hence this groove is probably also occupied by several carbohydrates of the N559-glycan und prompted us to analyse the glycan type at N559 by MS. Our LC-MS/MS analysis revealed a complex tetra antennary core-fucosylated N559-glycan (45% abundance) of which 13% comprise a bisecting GlcNAc comprising terminal Gal and GlcNAc added to the $GlcNAc_2(Fuc_1)Man_3$ core structure. Hence, the terminal Gal and GlcNAc can easily reach N905 and D1108 whereas the core Fuc might add additional hydrophobic interactions with either F953, H1064 and/or Y1066. In summary, the N559-glycan can establish extensive interactions within the groove built up i.a. by N905, H1064 and D1108 which most likely causes the slow dissociation rate k_d and results in the high affinity interaction with BoNT/A.

Limited knowledge about neuron specific N-glycan types is available and nothing is known about the type of N-glycans found in synaptic vesicle proteins. Therefore a comprehensive analysis of native SV proteins with respect to N-glycans should be performed. However, since our HEK cell-expressed gSV2CLD-Fc supports high affinity binding of BoNT/A we assume that mainly the $GlcNAc_2(Fuc_1)Man_3$ core structure of the N559-glycan contributes to recognition of BoNT/A whereas sugar moieties more distal to N559 probably protrude from the surface of H_CA and therefore do not or only transiently participate in the interaction. In contrast, the observed expanded bipartite interface in BoNT/E for the interaction with SV2A points towards a different glycan recognition by BoNT/E [28]. Ultimately, N559/573-glycan types of native SV2C and SV2A remain to be elucidated by LC-MS/MS methods and the interacting amino acids by structural approaches.

In conclusion, by means of recombinant eukaryotic expression of glycosylated SV2CLD we were able to demonstrate that BoNT/A exhibits a 12-fold higher affinity to glycosylated compared to non-glycosylated SV2C and identified the N559-glycan as being responsible.

Furthermore, this work provides insights into the mode of binding of BoNT/A to N-glycan structures. This detailed knowledge will be helpful for the development of multivalent binding inhibitors to prevent BoNT/A intoxications as well as of high affinity peptides to be employed in innovative detection systems to capture or enrich BoNT/A e.g. out of complex matrices.

ACKNOWLEDGEMENTS
We thank Nadja Krez for excellent technical assistance and Dr. Jasmin Weisemann for critical discussions and proof reading.

DECLARATIONS OF INTEREST
We declare no conflict of interest.

FUNDING
This work was supported in part by the Bundesministerium für Bildung und Forschung (BMBF) with grants FK 031A212A (A.R.) and FK 031A212B (B.G.D.) to the FuMiBoNT consortium. The work performed at FOI was supported by the Swedish Civil Contingencies Agency.

REFERENCES

1 Bigalke, H. and Rummel, A. (2005) Medical aspects of toxin weapons. Toxicology. **214**, 210-220

2 Arnon, S. S., Schechter, R., Inglesby, T. V., Henderson, D. A., Bartlett, J. G., Ascher, M. S., Eitzen, E., Fine, A. D., Hauer, J., Layton, M., Lillibridge, S., Osterholm, M. T., O'Toole, T., Parker, G., Perl, T. M., Russell, P. K., Swerdlow, D. L. and Tonat, K. (2001) Botulinum toxin as a biological weapon: medical and public health management. JAMA. **285**, 1059-1070

3 Bigalke, H. (2013) Botulinum toxin: application, safety, and limitations. Curr Top Microbiol Immunol. **364**, 307-317

4 Pirazzini, M., Rossetto, O., Bolognese, P., Shone, C. C. and Montecucco, C. (2011) Double anchorage to the membrane and intact inter-chain disulfide bond are required for the low pH induced entry of tetanus and botulinum neurotoxins into neurons. Cell Microbiol. **13**, 1731-1743

5 Fischer, A. (2013) Synchronized chaperone function of botulinum neurotoxin domains mediates light chain translocation into neurons. Curr Top Microbiol Immunol. **364**, 115-137

6 Pirazzini, M., Tehran, D. A., Leka, O., Zanetti, G., Rossetto, O. and Montecucco, C. (2016) On the translocation of botulinum and tetanus neurotoxins across the membrane of acidic intracellular compartments. Biochim Biophys Acta. **1858**, 467-474

7 Rummel, A. (2013) Double receptor anchorage of botulinum neurotoxins accounts for their exquisite neurospecificity. Curr Top Microbiol Immunol. **364**, 61-90

8 Rummel, A., Mahrhold, S., Bigalke, H. and Binz, T. (2004) The H_{CC}-domain of botulinum neurotoxins A and B exhibits a singular ganglioside binding site displaying serotype specific carbohydrate interaction. Mol Microbiol. **51**, 631-643

9 Stenmark, P., Dupuy, J., Imamura, A., Kiso, M. and Stevens, R. C. (2008) Crystal structure of botulinum neurotoxin type A in complex with the cell surface co-receptor GT1b-insight into the toxin-neuron interaction. PLoS Pathog. **4**, e1000129

10 Rummel, A., Häfner, K., Mahrhold, S., Darashchonak, N., Holt, M., Jahn, R., Beermann, S., Karnath, T., Bigalke, H. and Binz, T. (2009) Botulinum neurotoxins C, E and F bind gangliosides via a conserved binding site prior to stimulation-dependent uptake with botulinum neurotoxin F utilising the three isoforms of SV2 as second receptor. J Neurochem. **110**, 1942-1954

11 Dong, M., Richards, D. A., Goodnough, M. C., Tepp, W. H., Johnson, E. A. and Chapman, E. R. (2003) Synaptotagmins I and II mediate entry of botulinum neurotoxin B into cells. J Cell Biol. **162**, 1293-1303

12 Rummel, A., Karnath, T., Henke, T., Bigalke, H. and Binz, T. (2004) Synaptotagmins I and II act as nerve cell receptors for botulinum neurotoxin G. J Biol Chem. **279**, 30865-30870

13 Peng, L., Berntsson, R. P., Tepp, W. H., Pitkin, R. M., Johnson, E. A., Stenmark, P. and Dong, M. (2012) Botulinum neurotoxin D-C uses synaptotagmin I and II as receptors, and human synaptotagmin II is not an effective receptor for type B, D-C and G toxins. J Cell Sci. **125**, 3233-3242

14 Strotmeier, J., Willjes, G., Binz, T. and Rummel, A. (2012) Human synaptotagmin-II is not a high affinity receptor for botulinum neurotoxin B and G: increased therapeutic dosage and immunogenicity. FEBS Lett. **586**, 310-313

15 Takamori, S., Holt, M., Stenius, K., Lemke, E. A., Gronborg, M., Riedel, D., Urlaub, H., Schenck, S., Brugger, B., Ringler, P., Muller, S. A., Rammner, B., Grater, F., Hub, J. S., De Groot, B. L., Mieskes, G., Moriyama, Y., Klingauf, J., Grubmuller, H., Heuser, J., Wieland, F. and Jahn, R. (2006) Molecular anatomy of a trafficking organelle. Cell. **127**, 831-846

16 Janz, R. and Südhof, T. C. (1999) SV2C is a synaptic vesicle protein with an unusually restricted localization: anatomy of a synaptic vesicle protein family. Neuroscience. **94**, 1279-1290
17 Dong, M., Yeh, F., Tepp, W. H., Dean, C., Johnson, E. A., Janz, R. and Chapman, E. R. (2006) SV2 is the protein receptor for botulinum neurotoxin A. Science. **312**, 592-596
18 Dong, M., Liu, H., Tepp, W. H., Johnson, E. A., Janz, R. and Chapman, E. R. (2008) Glycosylated SV2A and SV2B mediate the entry of botulinum neurotoxin E into neurons. Mol Biol Cell. **19**, 5226-5237
19 Mahrhold, S., Rummel, A., Bigalke, H., Davletov, B. and Binz, T. (2006) The synaptic vesicle protein 2C mediates the uptake of botulinum neurotoxin A into phrenic nerves. FEBS Lett. **580**, 2011-2014
20 Fu, Z., Chen, C., Barbieri, J. T., Kim, J. J. and Baldwin, M. R. (2009) Glycosylated SV2 and gangliosides as dual receptors for botulinum neurotoxin serotype F. Biochemistry. **48**, 5631-5641
21 Peng, L., Tepp, W. H., Johnson, E. A. and Dong, M. (2011) Botulinum Neurotoxin D Uses Synaptic Vesicle Protein SV2 and Gangliosides as Receptors. PLoS Pathog. **7**, e1002008
22 Yeh, F. L., Dong, M., Yao, J., Tepp, W. H., Lin, G., Johnson, E. A. and Chapman, E. R. (2010) SV2 mediates entry of tetanus neurotoxin into central neurons. PLoS Pathog. **6**, e1001207
23 Bercsenyi, K., Schmieg, N., Bryson, J. B., Wallace, M., Caccin, P., Golding, M., Zanotti, G., Greensmith, L., Nischt, R. and Schiavo, G. (2014) Tetanus toxin entry. Nidogens are therapeutic targets for the prevention of tetanus. Science. **346**, 1118-1123
24 Strotmeier, J., Gu, S., Jutzi, S., Mahrhold, S., Zhou, J., Pich, A., Eichner, T., Bigalke, H., Rummel, A., Jin, R. and Binz, T. (2011) The biological activity of botulinum neurotoxin type C is dependent upon novel types of ganglioside binding sites. Mol Microbiol. **81**, 143-156
25 Weisemann, J., Stern, D., Mahrhold, S., Dorner, B. G. and Rummel, A. (2016) Botulinum Neurotoxin Serotype A Recognizes Its Protein Receptor SV2 by a Different Mechanism than Botulinum Neurotoxin B Synaptotagmin. Toxins (Basel). **8**
26 Benoit, R. M., Frey, D., Hilbert, M., Kevenaar, J. T., Wieser, M. M., Stirnimann, C. U., McMillan, D., Ceska, T., Lebon, F., Jaussi, R., Steinmetz, M. O., Schertler, G. F., Hoogenraad, C. C., Capitani, G. and Kammerer, R. A. (2014) Structural basis for recognition of synaptic vesicle protein 2C by botulinum neurotoxin A. Nature. **505**, 108-111
27 Strotmeier, J., Mahrhold, S., Krez, N., Janzen, C., Lou, J., Marks, J. D., Binz, T. and Rummel, A. (2014) Identification of the synaptic vesicle glycoprotein 2 receptor binding site in botulinum neurotoxin A. FEBS Lett. **588**, 1087-1093
28 Mahrhold, S., Strotmeier, J., Garcia-Rodriguez, C., Lou, J., Marks, J. D., Rummel, A. and Binz, T. (2013) Identification of the SV2 protein receptor-binding site of botulinum neurotoxin type E. Biochem J. **453**, 37-47
29 Weisemann, J., Krez, N., Fiebig, U., Worbs, S., Skiba, M., Endermann, T., Dorner, M., Bergström, T., Munoz, A., Zegers, I., Müller, C., Jenkinson, S., Avondet, M.-A., Delbrassinne, L., Denayer, S., Zeleny, R., Schimmel, H., Astot, C., Dorner, B. and Rummel, A. (2015) Generation and Characterization of Six Recombinant Botulinum Neurotoxins as Reference Material to Serve in an International Proficiency Test. Toxins (Basel). **7**, 4861
30 Bergström, T., Fredriksson, S. A., Nilsson, C. and Astot, C. (2015) Deamidation in ricin studied by capillary zone electrophoresis- and liquid chromatography-mass spectrometry. J Chromatogr B. **974**, 109-117
31 Myszka, D. G. (1999) Improving biosensor analysis. J Mol Recognit. **12**, 279-284

32 Bateman, K. P., White, R. L. and Thibault, P. (1998) Evaluation of adsorption preconcentration/capillary zone electrophoresis/nanoelectrospray mass spectrometry for peptide and glycoprotein analyses. J Mass Spectrom. **33**, 1109-1123
33 Kwon, S. E. and Chapman, E. R. (2012) Glycosylation is dispensable for sorting of synaptotagmin 1 but is critical for targeting of SV2 and synaptophysin to recycling synaptic vesicles. J Biol Chem. **287**, 35658-35668
34 Han, W., Rhee, J. S., Maximov, A., Lao, Y., Mashimo, T., Rosenmund, C. and Sudhof, T. C. (2004) N-glycosylation is essential for vesicular targeting of synaptotagmin 1. Neuron. **41**, 85-99
35 Torii, T., Yoshimura, T., Narumi, M., Hitoshi, S., Takaki, Y., Tsuji, S. and Ikenaka, K. (2014) Determination of major sialylated N-glycans and identification of branched sialylated N-glycans that dynamically change their content during development in the mouse cerebral cortex. Glycoconj J. **31**, 671-683
36 von Der Ohe, M., Wheeler, S. F., Wuhrer, M., Harvey, D. J., Liedtke, S., Muhlenhoff, M., Gerardy-Schahn, R., Geyer, H., Dwek, R. A., Geyer, R., Wing, D. R. and Schachner, M. (2002) Localization and characterization of polysialic acid-containing N-linked glycans from bovine NCAM. Glycobiology. **12**, 47-63
37 Saphire, E. O., Parren, P. W., Pantophlet, R., Zwick, M. B., Morris, G. M., Rudd, P. M., Dwek, R. A., Stanfield, R. L., Burton, D. R. and Wilson, I. A. (2001) Crystal structure of a neutralizing human IGG against HIV-1: a template for vaccine design. Science. **293**, 1155-1159
38 Nishima, W., Miyashita, N., Yamaguchi, Y., Sugita, Y. and Re, S. (2012) Effect of bisecting GlcNAc and core fucosylation on conformational properties of biantennary complex-type N-glycans in solution. J Phys Chem B. **116**, 8504-8512

TABLES

Table 1. Peptides identified in gSV2CLD-Fc wild-type by LC-MS. Amino acid numbering according to SV2C wild-type sequence.

No.	Tryptic peptides from gSV2CLD-Fc wild-type	SV2C AA number		Peptide mass [Da]	Most abundant ion [*m/z*]	Most abundant glycan
		Start	End			
1	DSVFK	514	518	594.30	595.3^{1+}	
2	SC*TFEDVTSVNTYFK	519	533	1796.79	599.9^{3+}	
3	N_{glyco}C*TFIDTVFDNTDFEPYK	534	551	3644.50[a]	1215.8^{3+}	$GlcNAc_3Hex_5$
4	FIDSEFK	552	558	884.43	443.2^{2+}	
5	**N**C*SFFHNK	559	566	1052.45	351.8^{3+}	
6	**N_{glyco}**C*SFFHN$_{glyco}$K	559	566	5320.09[a]	1331.2^{4+}	$2x(GlcNAc_2Fuc_1Man_3GlcNAc_3Gal_3)$
7	FIDSEFK**N_{glyco}**C*SFFHN$_{glyco}$K	552	566	6916.79[a]	1384.6^{5+}	$2x(GlcNAc_2Fuc_1Man_3GlcNAc_4Gal_4)$
8	TGC*QITFDDDYSA*PGSAWSHPQFEK*[#]	567	579	2843.21	948.7^{3+}	

AA 559 in bold, N_{glyco}=glycosylated asparagine, C*=carbamidomethylated cysteine, GlcNAc=N-acetylglucosamine, Man=mannose, Glc=glucose, Fuc=fucose, Hex=hexose, [a]=heterogeneous glycosylation, calculation made using the most abundant glycoform, [#]residues in italic are part of the C-terminally fused Streptag

Table 2. Binding kinetics and affinity of recombinant H_CA to immobilized gSV2CLD-Fc wild-type and gSV2CLD-Fc mutant as determined by SPR. Shown are mean values ± standard deviations of two technical replicates. Binding kinetics were determined by fitting the double referenced binding curves using the 1:1 Langmuir binding model.

Ligand	k_a [$M^{-1}s^{-1}$]	k_d [s^{-1}]	K_D [M]
gSV2CLD-Fc wild-type	$2.1 \pm 0.5 \times 10^4$	$2.2 \pm 0.4 \times 10^{-3}$	$1.1 \pm 0.0 \times 10^{-7}$
gSV2CLD-Fc N559A	$8 \pm 3 \times 10^4$	$1.1 \pm 0.8 \times 10^{-1}$	$1.3 \pm 0.5 \times 10^{-6}$

FIGURES

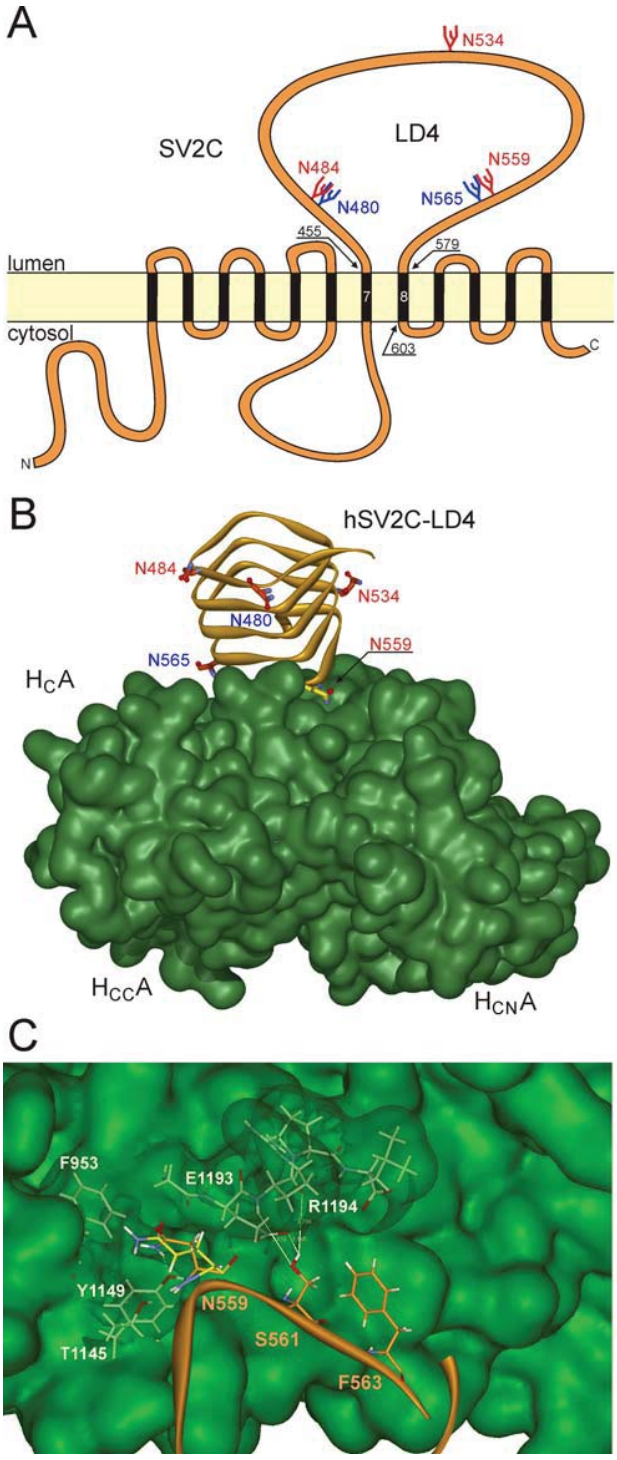

Figure 1. Topology of SV2C and binding of non-glycosylated hSV2C-LD4 to BoNT/A H_C. **(A)** Schematic representation of the membrane topology of SV2C. SV2C spans the membrane of synaptic vesicles twelve times. N- and carboxyl-termini are located on the cytosolic face, while the LD4 between transmembrane regions seven and eight is located on the luminal face of the synaptic vesicle membrane. The three PNG sites of the LD4 conserved throughout SV2

isoforms and species are highlighted in red. SV2C contains two additional PNG sites which are shown in blue. (**B)** Co-crystal structure of non-glycosylated hSV2C-LD4 (yellow ribbon) bound to H_CA (green surface; [26], 4JRA.pdb). Asparagines of PNG sites are highlighted in red stick representation. N559 homologous to N573 of SV2A important for BoNT/E binding is located in close proximity to H_CA (yellow stick representation). **(C)** Close-up view of the SV2C-H_CA binding interface. The SV2C residues N559 and S561 (shown as sticks with orange carbons) interact via H-bonds with T1145/Y1149 and E1193/R1194 of H_CA (green), respectively. Mutation S561A removes the serine hydroxyl-group thereby breaking H-bonds to E1193/R1194. Mutation N559Q (Q559 in sticks with yellow carbons) moves the amide group away from T1145/Y1149 of H_CA also resulting in loss of H-bonds and additionally interfering with the phenyl ring of F953.

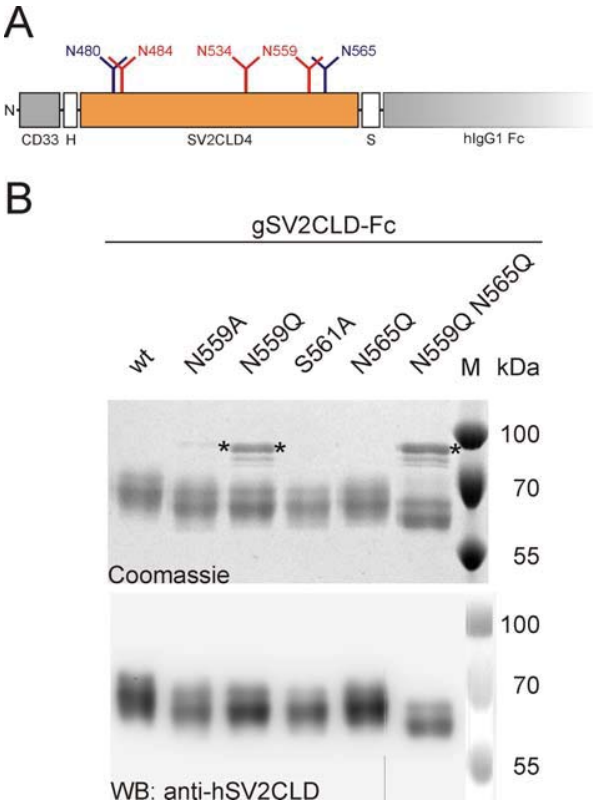

Figure 2. Expression and purification of gSV2CLD-Fc in HEK cells.
(A) Schematic representation of the DNA construct used for the expression of gSV2CLD-Fc in HEK cells. The amino-terminal CD33 signal peptide directs the translation of the polypeptide for post-translational glycosylation into the ER and Golgi apparatus and final secretion into the cell culture medium. His6- (H) and Strep-tags (S) allow the tandem affinity purification of the secreted proteins from cell culture supernatants. The hIgG1 Fc facilitates efficient secretion, glycosylation and folding and allows the immobilization of the fusion proteins on protein G-sepharose matrix for the use in pull down experiments. The conserved PNG sites are highlighted in red, while the additional non-conserved PNG sites of SV2C are highlighted in blue. **(B)** Representative SDS-PAGE (top) and Western Blot (bottom) analysis of ~750 ng gSV2CLD-Fc wild-type and gSV2CLD-Fc mutants. Protein bands were visualized by Coomassie Blue staining. Protein species comprising the human SV2C LD4 peptide were identified by Western Blot analysis employing the rabbit anti-human SV2C LD4 polyclonal antibody. The detected apparent molecular weight (approximately 60 kDa) was much higher compared to the calculated molecular weight (approximately 46 kDa) of the peptide backbone, indicating that the fusion proteins are glycosylated in HEK cells. Asterisks (*) denote residual impurities which mainly derive from bovine serum albumin used in the cell culture media.

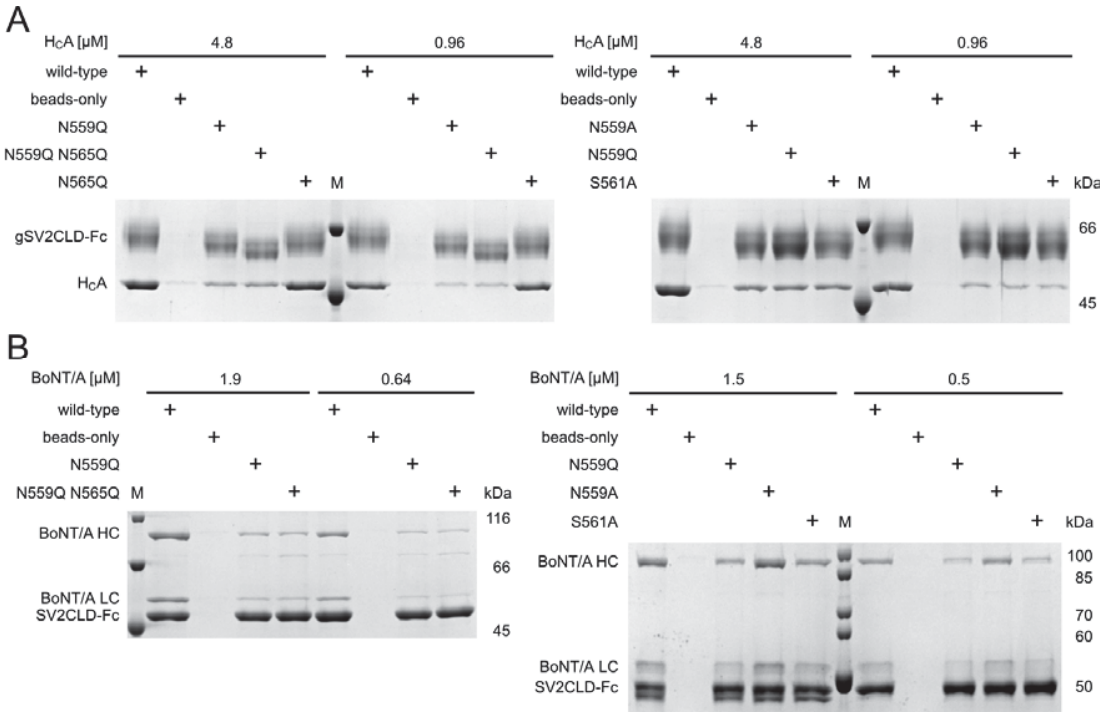

Figure 3. Binding of H_CA and BoNT/A to gSV2CLD-Fc and bacterial SV2CLD-Fc wild-type and mutants. 100 pmol of glycosylated **(A)** or non-glycosylated **(B)** wild-type and mutant hSV2CLD-Fc were immobilized to protein G-sepharose matrix and incubated with the indicated concentrations of H_CA **(A)** or BoNT/A **(B)**, respectively, in a total volume of 200 µL. After removal of supernatant and washing of the beads, bound proteins were visualized by SDS-PAGE and Coomassie Blue staining.

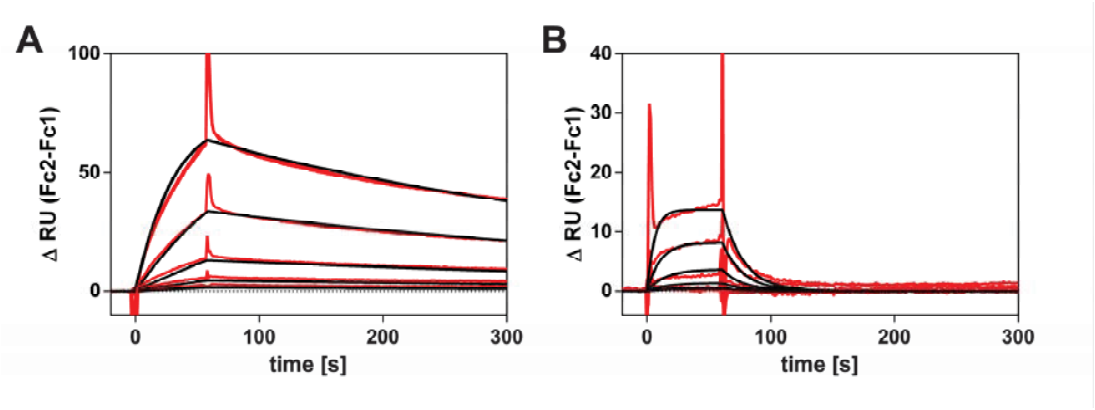

Figure 4. Surface plasmon resonance analysis of the binding of gSV2CLD-Fc wild-type and gSV2CLD-Fc N559A mutant to H_CA. Double referenced (ΔRU) sensorgrams for binding of recombinant H_CA (1800 nM to 22.2 nM; red) to immobilized gSV2CLD-Fc wild-type (**A**) or gSV2CLD-Fc N559A (**B**) were fitted to a 1:1 Langmuir interaction model (black) to determine binding kinetics and affinity.

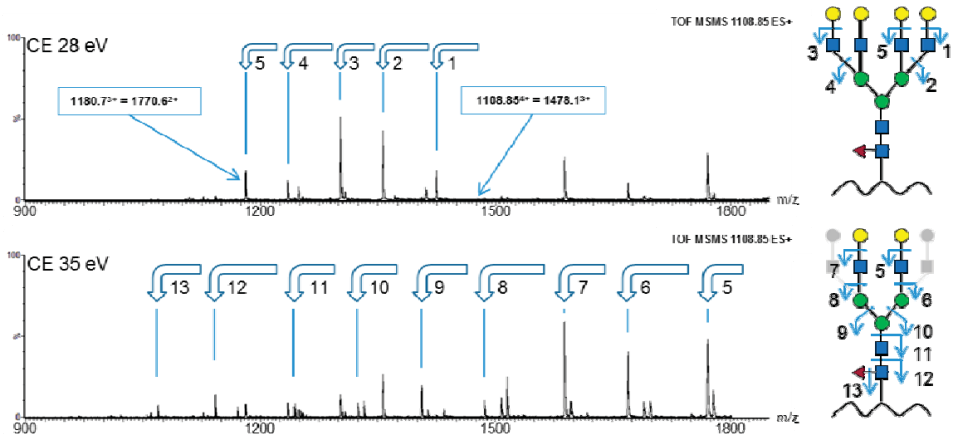

Figure 5. Product ion spectra of the $F^{552}IDSEFKN_{glyco}C^{*}SFFHQK^{566}$ peptide of the gSV2CLD-Fc N565Q mutant using collision energies of 28 eV (top) and 35 eV (bottom) displaying the tetra antennary, core-fucosylated N559-glycan structure. At intermediate collision energy the loss of terminal galactoses (yellow circle) and GlcNAcs (blue square) was detected (top). At higher collision energy, the subsequent fragmentation of tri-mannose (green circle), fucose (red triangle) and GlcNAc (blue square) of the core structures was observed (bottom).

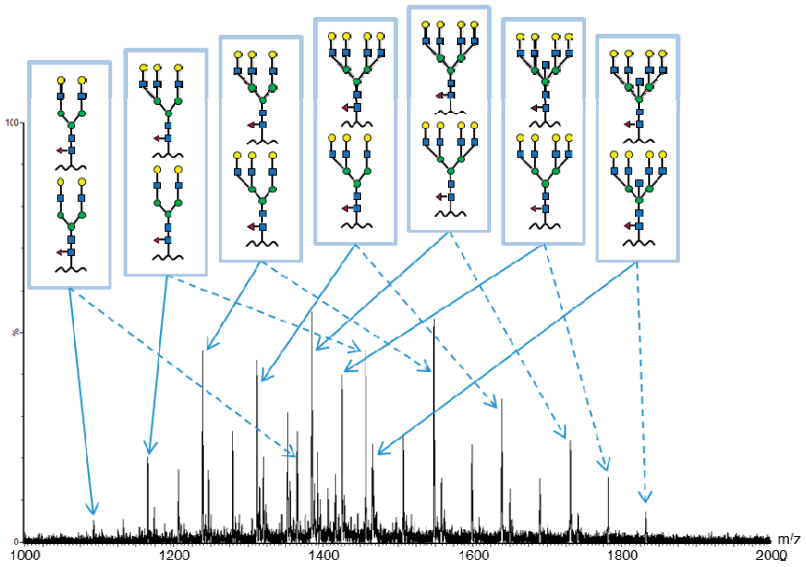

Figure 6. Mass spectrum of the $F^{552}IDSEFKN_{glyco}C^{*}SFFHN_{glyco}K^{566}$ peptide from the gSV2CLD-Fc wild-type construct showing the large glycan heterogeneity at N559 and N565, detected in both the $[M+4H]^{4+}$ (dashed arrow) and $[M+5H]^{5+}$ (solid arrow) charge states. Annotations: yellow circle = galactose, blue square = N-acetylglucosamine, green circle = mannose and red triangle = fucose.